



# Magnetism in $\text{BiFe}_{1-x}\text{Ni}_x\text{O}_3$ : studied through electron spin resonance spectroscopy

M. R. Biswal<sup>1</sup> · J. Nanda<sup>2</sup> · N. C. Mishra<sup>3</sup> · S. S. Acharya<sup>4</sup> · D. K. Mishra<sup>2</sup> · V. V. Srinivasu<sup>5</sup>

Received: 12 June 2018 / Accepted: 9 October 2018 / Published online: 11 October 2018  
© Springer Science+Business Media, LLC, part of Springer Nature 2018

## Abstract

The effect of Ni doping in  $\text{BiFe}_{1-x}\text{Ni}_x\text{O}_3$  (BFNO) multiferroics are studied by X-ray diffraction (XRD), Fourier transmission infrared (FTIR) spectroscopy, X-ray photoelectron spectroscopy (XPS), hysteresis loop (M–H), temperature dependent magnetization (FC-ZFC) measurements and electron spin resonance (ESR) techniques. The XRD and FTIR studies indicate that the BFNO compounds remain in rhombohedral (R3c) phase without appearance of any structural transformation due to Ni doping. The XPS studies show the oxidation states of Fe ions as  $3^+$ , whereas Bi is found to be in a mixed valence state of  $2^+$  and  $3^+$  in BFNO. The Ni ion doping enhances the saturation magnetization from 0.179 emu/g ( $x=0.025$ ) to 2.38 emu/g ( $x=0.20$ ), which is higher than the reported values found in literature. The FC-ZFC magnetization studies suggest the presence of a magnetic phase transition from a weak ferromagnetic to a spin glass state at low temperature. The ESR studies confirm the ferromagnetic state of BFNO samples.

## 1 Introduction

Bismuth ferrite has been widely studied for the past two decades. It exhibits multiferrocity at room temperature and has immense applications in multifunctional devices such as actuators, transducers, spin valves, data storage, solar cells, supercapacitors, medicine and so on [1–6]. This multiferroic has also created a platform for the physicists to reveal the fundamental physics. Bismuth ferrite ( $\text{BiFeO}_3$ ) has been synthesized as bulk [7–10], nanopowder [11, 12], thin films [13, 14] and nonflowers [15]. Bismuth ferrite (BFO) has

a rhombohedrally distorted perovskite structure with space group R3c. BFO is also a magnetoelectric material exhibiting a weak coupling between the electric polarization and magnetization [16]. The pristine BFO is known to be ferroelectric below 1100 K and antiferromagnetic with a Neel temperature of 640 K. BFO exhibits spin cycloid structure with a modulated wavelength of 62 nm [10]. Neutron diffraction studies confirmed the antiferromagnetic ordering of G-type, where every atom is surrounded by six atoms with oppositely oriented spins. The magnetic moments of iron ions rotate along the propagation direction of the modulated wave in the plane perpendicular to the hexagonal basal plane. A weak ferromagnetism has also been predicted using the first-principles density functional theory [17].

Transition metal doping influences the magnetic and magnetoelectric coupling behaviour of bismuth ferrite by locally modifying the magnetic interaction [18–20]. Transition metal ion substitution at B site has been proved to be effective in inducing room temperature ferromagnetization in BFO. Hence, there is a persistent effort to improve its magnetic properties by suitable doping of transition metal ions at B site. The substitution of  $\text{Ni}^{2+}$  ion at  $\text{Fe}^{3+}$  site mostly creates oxygen vacancies to compensate the charge imbalance. Hence, it has been observed that substituting nickel ions at Fe site of BFO enhances the leakage current of the parent compound [21]. Nevertheless, the substitution of Ni at Fe site can enhance magnetization due to strong

✉ J. Nanda  
jyotirmayeenanda@soa.ac.in

<sup>1</sup> Department of Physics, Hi-Tech Engineering College, Bhubaneswar, Odisha 752054, India

<sup>2</sup> Department of Physics, Faculty of Engineering and Technology (ITER), Siksha 'O' Anusandhan (Deemed to be University), Khandagiri Square, Bhubaneswar, Odisha 751030, India

<sup>3</sup> Department of Physics, Utkal University, Bhubaneswar, Odisha 751004, India

<sup>4</sup> Institute of Physics, Sachivalaya Marg, Bhubaneswar, Odisha 751005, India

<sup>5</sup> Department of Physics, College of Science, Engineering and Technology, University of South Africa, 1710 Johannesburg, South Africa

ferromagnetic interaction between  $\text{Fe}^{3+}$  and  $\text{Ni}^{2+}$  under  $180^\circ$  superexchange interaction. Amit et al. [22] have reported increase in magnetization with increasing Ni concentration in BFO. The authors, however, observed Superparamagnetism in nanoparticles of Ni doped BFO. Besides, Wang et al. [23] have reported the enhancement of magnetization of BFO when Ni doping concentration increases to 0.5%. Further, the magnetization of nanocrystalline Ni-doped BFO (10%) has been reported to increase as compared to pristine BFO [24]. According to Wang and Qi [25], the observed ferromagnetic behaviour is either due to the reduction of  $\text{Fe}^{3+}$  to  $\text{Fe}^{2+}$  or increase in the canting angle. The increase in magnetization with Ni substitution has also been reported by Kharel et al. [26] for Ni doped BFO films deposited on Si (100) substrates.

To the best of our knowledge, there is hardly any report on the magnetic properties of Ni-doped BFO, explored by SQUID (FC and ZFC) and ESR spectroscopy. This paper presents a detail study on both BFO and nickel doped BFO compounds, synthesized by solid-state reaction route. We employed XRD, XPS, FTIR spectroscopy, room temperature and low temperature magnetic hysteresis studies, FC-ZFC magnetic measurements and ESR studies. This study indicates a transformation of the antiferromagnetic state of BFO to a weak ferromagnetic one in BFNO. The ESR study clearly confirms the existence of ferromagnetic states in these multiferroics.

## 2 Experimental

The pristine BFO ( $\text{BiFeO}_3$ ) and BFNO  $\{\text{BiFe}_{1-x}\text{Ni}_x\text{O}_3$  ( $0.00 \leq x \leq 0.20$ )\} were prepared by conventional solid state reaction route. Stoichiometric amounts of high-purity dried oxide reagents  $\text{Bi}_2\text{O}_3$ ,  $\text{Fe}_2\text{O}_3$ , and NiO (analytical grade with purity  $\geq 99.9$ ) were mixed and ground thoroughly through ethanol medium for 2 h to get a homogeneous mixture and subsequently calcined at  $800^\circ\text{C}$  for 2 h through rapid heating. The calcined powders were pelletized in the form of circular discs using PVA as binder. The pressed pellets were sintered at  $800^\circ\text{C}$  for 2 h by rapid heating. The XRD patterns of samples were examined using Bruker D8 Advance X-ray diffractometer with  $\text{Cu-K}\alpha$  radiation. The FTIR spectra of the samples were recorded on a Bomem spectrophotometer, model MB-100. The X-ray photoelectron spectroscopy (XPS) studies have been carried out in a vacuum of  $10^{-10}$  torr using VSW ESCA machine (Analyzer model HAS 300) equipped with hemispherical analyzer, dual anode X-ray source and argon ion sputter gun. The magnetic properties (hysteresis loops at room temperature and temperature dependent magnetization curves) were studied by using a MPMS SQUID VSM Ever Cool system. For Electron Spin Resonance (ESR) measurements of samples, a commercial

X-band ( $f \approx 9.37$  GHz) Bruker EMXplus model spectrometer was used.

## 3 Results and discussion

The XRD analysis, microstructural studies by scanning electron microscope and electrical properties of BFO and BFNO have been reported in our previous publication [27]. XRD studies show that the rhombohedral distorted perovskite structure of the parent compound has been retained even with increase in Ni concentration upto 15%. The surface morphology of the samples was studied through SEM, which revealed the average grain size of the order of  $0.5\ \mu\text{m}$ .

### 3.1 Fourier transform infrared spectroscopy studies

The room temperature FTIR spectra of BFO and BFNO samples are displayed in Fig. 1.

A few absorption bands along with a curvature (from  $1000$  to  $2000\ \text{cm}^{-1}$ ) are seen in the FTIR spectrum. The curvature is a characteristic feature of semiconducting materials [28]. The typical band characteristics of metal oxygen bond were observed. The peaks observed at around  $813\ \text{cm}^{-1}$  and  $1074\ \text{cm}^{-1}$  are due to carbonate groups [29]. The absorption peak at around  $577\ \text{cm}^{-1}$  corresponds to Fe–O band stretching in the perovskite structure due to O–Fe–O bending of  $\text{FeO}_6$  group. The result is consistent with the characteristic infrared absorption bands of BFO [30]. The broad nature of the observed vibration band at about  $577\ \text{cm}^{-1}$  is attributed to the occurrence of absorption peaks of both iron and bismuth oxide at nearly same wave number. Another absorption peak of  $\text{FeO}_6$  octahedral structure is also seen at around  $537\ \text{cm}^{-1}$ . Bhusan et al. [31] have reported the increase in relative intensities of these two peaks with increase in doping concentration, which indicates that FTIR measurements can be quite useful in confirming Ni substitution in BFO. However, there is no observation of increase in relative intensity of these two bands in our samples. We have noticed the shifting of these two bands towards higher frequencies with the increase in doping concentration.

### 3.2 X-ray photoelectron spectroscopic studies

Furthermore, XPS study was carried out for BFO and BFNO samples to determine the electronic state of Bi, Fe, Ni and O. The spectra were calibrated with the core-level peak at  $204.6\ \text{eV}$  of C 1s. The survey scan of BFNO sample does not show any peak corresponding to Ni ion as the XPS scan is done only on the surface of the samples and it indicates that Ni is not present on the surface of the BFNO samples. The narrow energy window scans along with the fitted curves are displayed in Fig. 2 for Bi and Fe. Core levels have been

**Fig. 1** FTIR spectra of  $\text{BiFe}_{1-x}\text{Ni}_x\text{O}_3$  ( $0.00 \leq x \leq 0.20$ ) samples

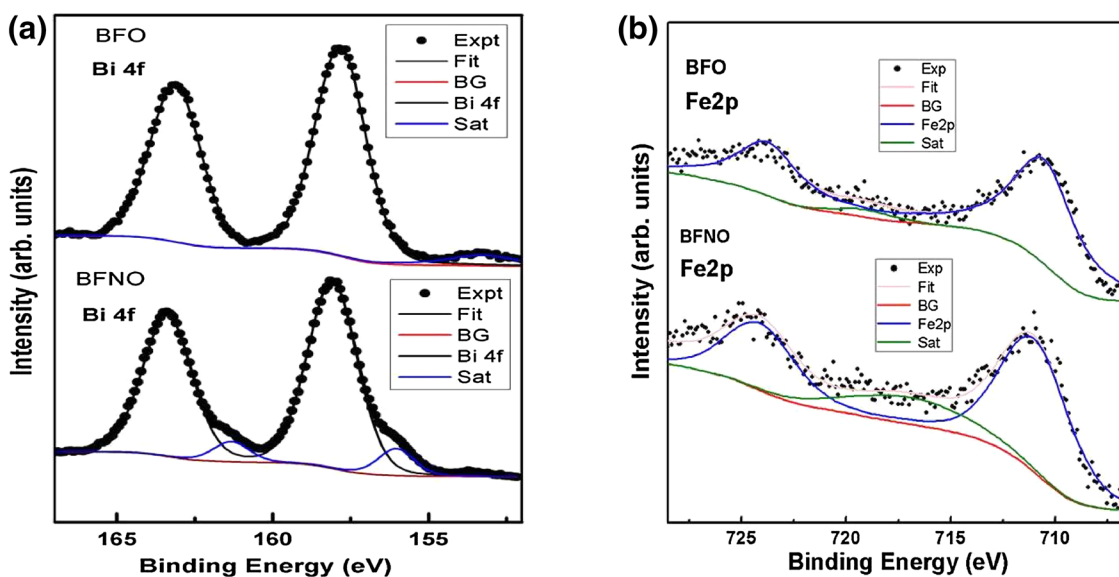
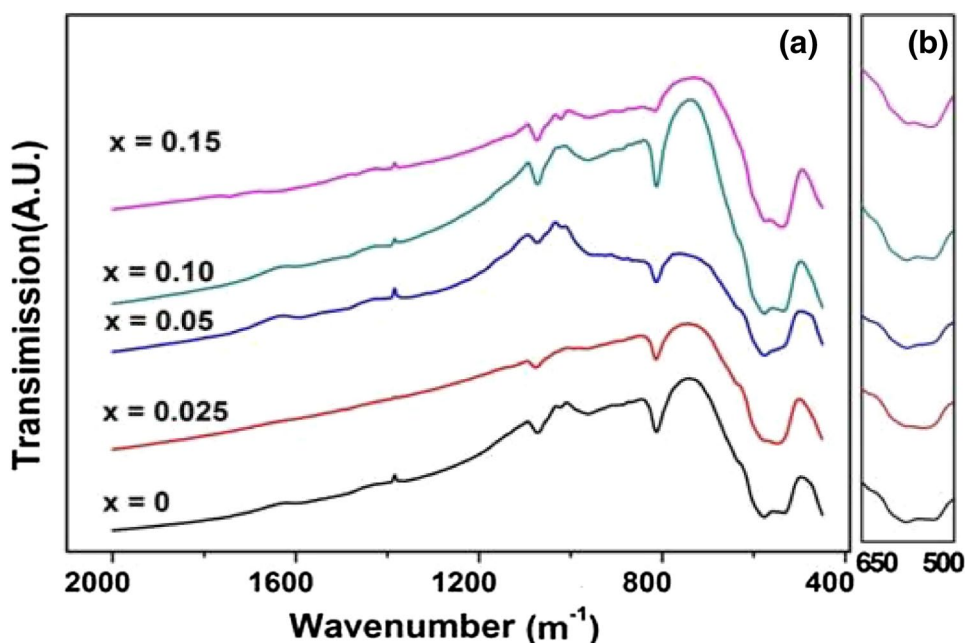


**Fig. 2** The XPS spectra along with the fitted curves for the core energy levels of **a** Bi 4*f*, and **b** Fe 3*d* for  $\text{BiFeO}_3$  and  $\text{BiFe}_{1-x}\text{Ni}_x\text{O}_3$  ( $x=0.075$ ) samples

analyzed using XPS PEAK fitting software [32] with Gaussian–Lorentzian sum function. Shirley algorithm was used for background correction.

As shown in Fig. 2a, the main  $4f_{7/2}$  peak occurs at 157.8 eV and 158.1 eV for BFO and BFNO samples and the corresponding  $4f_{5/2}$  features occur at 163.1 eV and 163.4 eV. At around 153.5 eV B.E. a X-ray satellite peak corresponding to Al  $K\alpha_{3,4}$  (from detector) is observed. Interestingly, low binding energy (B.E.) feature is observed at around 156 eV for Bi 4*f* of BFNO, which may correspond to a lower valence

state of Bi on the surface. Mishra et al. [33] have observed a peak at 162.49 eV ( $4f_{5/2}$ ) corresponding to lower valence state of bismuth ion, in addition to the peak at 164.56 eV for the dominant trivalent  $\text{Bi}^{3+}$  in Ni-doped BFO films. Fe 2*p* spectra of BFO and BFNO are shown in Fig. 2b. Fe  $2p_{3/2}$  feature occurs at 710.5 eV and 711 eV respectively for BFO and BFNO, whereas Fe  $2p_{1/2}$  levels are seen at 723.7 eV and 724.2 eV for BFO and BFNO respectively. Some shake-up satellites are also observed at higher B.E. These binding energies are characteristics of  $\text{Fe}^{3+}$  ions [34]. Similar

spin orbit doublet components of Fe 2*p* lines for BFO and doped BFO samples have been reported by several authors [26, 35–38]. Xu et al. [36] also observed a satellite peak at around 718.6 eV for their Bi<sub>0.9</sub>Dy<sub>0.1</sub>FeO<sub>3</sub> powder. From XPS measurements, it is concluded that Fe is predominantly in the 3+ valence state for both BFO and BFNO. The asymmetric peaks of Fe spectrum may also be fitted with two peaks corresponding to Fe<sup>3+</sup> and Fe<sup>2+</sup> states. But the analysis predicts the predominant existence of Fe<sup>3+</sup> states [39]. Hence, we do believe that the magnetic properties of our samples are mainly dominated by Fe<sup>3+</sup> states.

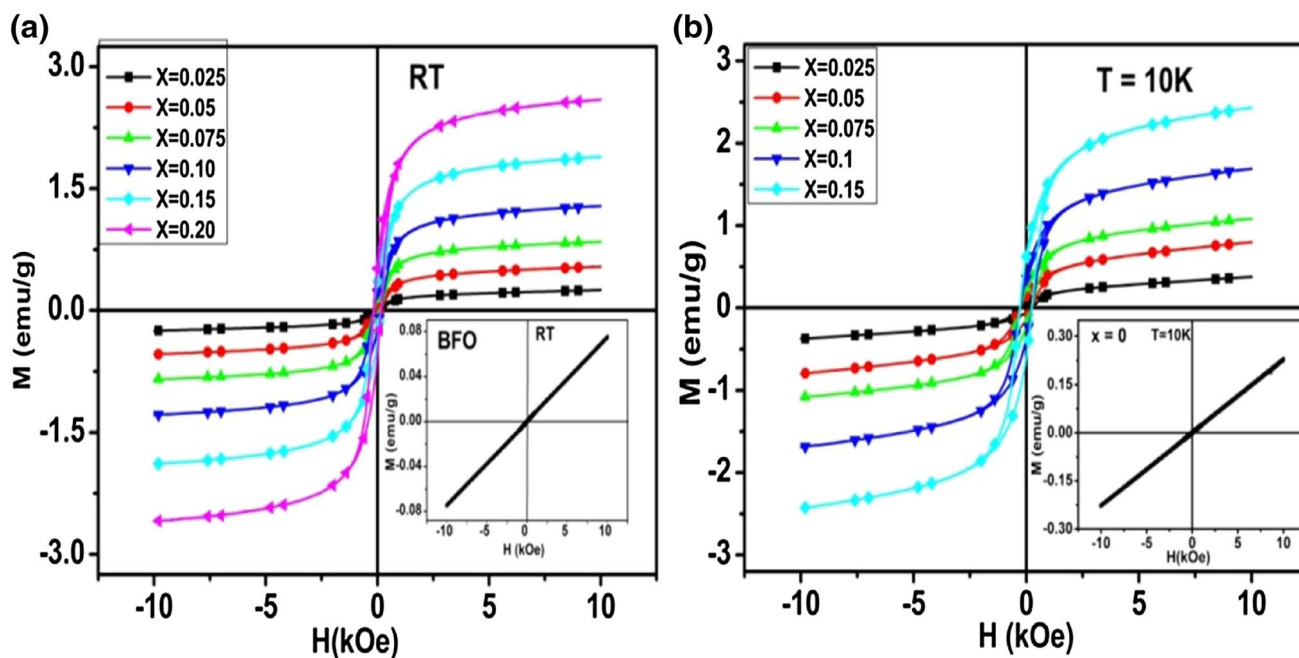
### 3.3 Magnetic studies

Figure 3a and b display the hysteresis loops of BiFe<sub>1-x</sub>Ni<sub>x</sub>O<sub>3</sub> (0.00 ≤ *x* ≤ 0.20) samples recorded at 300 K (RT) and 10 K respectively. It is observed that, saturation is not achieved in all the samples for an applied DC magnetic field of < 10 kOe. Hence, the saturation magnetization (*M<sub>s</sub>*) values were found out by extrapolating the loop from the high field to zero field. The *M*–*H* loops of BFO (at 10 and 300 K) are displayed as insets to Fig. 3a, b. The magnetic hysteresis loops show nearly linear field dependence and do not exhibit any tendency of saturation. This indicates the antiferromagnetic nature of BFO, which originates from the antiferromagnetic alignment of Fe moments between adjacent (111) planes [18].

To see the effect of Ni doping, the saturation magnetization (*M<sub>s</sub>*), remanant magnetization (*M<sub>r</sub>*), and coercivity

(*H<sub>c</sub>*) values of BFO and BFNO are plotted. As shown in Fig. 4a, *M<sub>s</sub>* increases rapidly from 0.179 to 2.383 emu/g with increasing Ni ion concentration from 0.025 to 0.20. This value is larger than that reported earlier for Ni substituted BFO samples [23, 40]. The enhancement of magnetization with increase in Ni concentration may be due to the possible double exchange interactions of Fe and Ni. The *H<sub>c</sub>* values did not change much with the increase in Ni concentration, except a shallow dip at a Ni conc. of 7.5%. As shown in Fig. 4, the *M<sub>s</sub>* and *M<sub>r</sub>* values showed a minimal increase with the lowering of temperature, whereas the *H<sub>c</sub>* values showed a substantial increase at 10 K attaining a value of 260 Oe.

The FC and ZFC magnetization curves of the BFO and BFNO samples are displayed in Fig. 5. As shown in Fig. 5a, the ZFC and FC curves merges with each other (throughout the temperature range of 10–300 K), which indicates the typical paramagnetic nature of BFO. The temperature dependent DC magnetization curves ranging from 5–300 K for BFNO are displayed in Fig. 5b–f. Both FC and ZFC curves have been traced for BFO and BFNO samples at an applied field of 1 kOe. The FC curves showed quasi-Brillouin dependence with temperature. The splitting exhibits an irreversible thermo-magnetization process. This type of behavior has been observed by Kharel et al. [26] for transition metal doped BFO thin films, where they have commented that this type of behavior is an indication of the presence of nano-scale magnetic secondary phases. They have also ruled out the possibility of magnetization contributions



**Fig. 3** Magnetic field dependent magnetization curves of BiFe<sub>1-x</sub>Ni<sub>x</sub>O<sub>3</sub> (0.00 ≤ *x* ≤ 0.20) samples recorded at **a** *T* = 300 K and **b** 10 K. Inset shows the *M*–*H* curves of BiFeO<sub>3</sub> sample; **a** *T* = 300 K and **b** 10 K

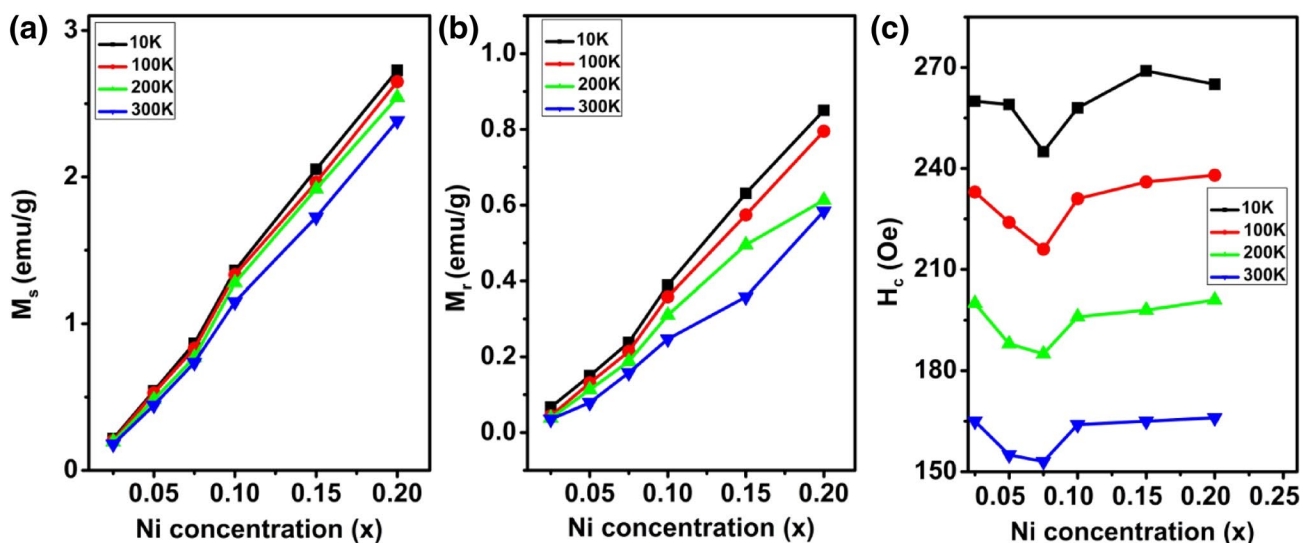


Fig. 4 Effect of Ni doping on a saturation magnetization, (M<sub>s</sub>), b remanant magnetization, (M<sub>r</sub>), and c coercivity, (H<sub>c</sub>) in BiFe<sub>1-x</sub>Ni<sub>x</sub>O<sub>3</sub> (0.00 ≤ x ≤ 0.20) samples. (The points are joined by lines for visual clarity)

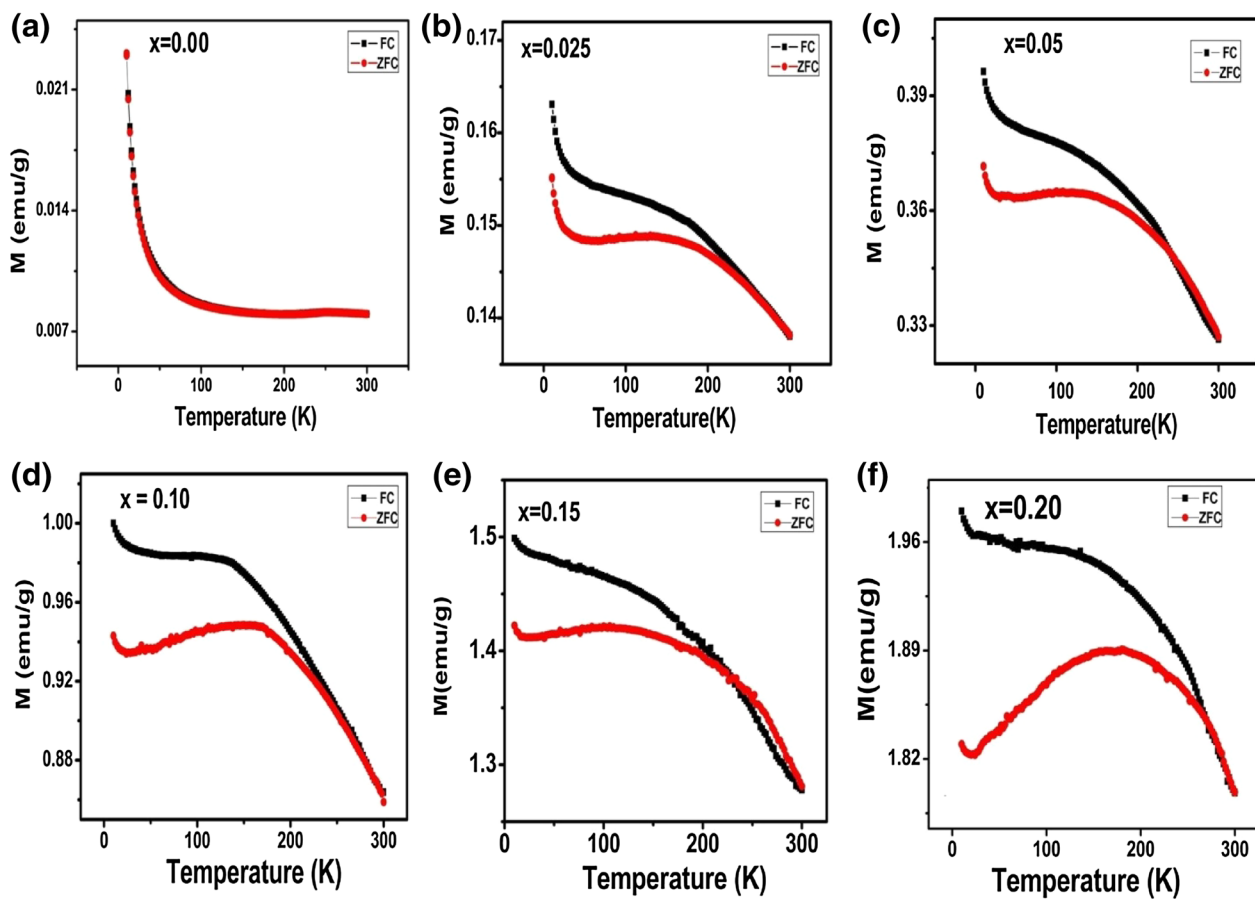


Fig. 5 Temperature dependence of magnetization of BiFe<sub>1-x</sub>Ni<sub>x</sub>O<sub>3</sub> (0.00 ≤ x ≤ 0.20) samples

from the impurities, which are usually seen in the XRD patterns of BFO samples.

The ZFC curves of the BFNO samples are found to be bifurcated from the corresponding FC curves due to an irreversible thermo magnetization process, which increase gradually till  $x=0.2$ . A prominent Curie tail is observed in all the samples. This type of tail was observed by Das et al. [41] for BFO samples. They have explained this as an indication of the presence of undetected paramagnetic impurity. Two impurity phases have been detected in the XRD pattern of our samples. Hence, this tail may be attributed to the presence of  $\text{Bi}_{25}\text{FeO}_{40}$ . The ZFC curves showed a prominent peak called as the spin-glass transition temperature. FC magnetization values remain almost constant or decrease with temperature below spin glass transition temperature ( $T_g$ ), which is characteristics of spin glass [42].

In some cases, the random interaction between the cluster of magnetic spins results in a state which is highly irreversible and metastable, known as the spin glass state [43]. Moreover, the ferromagnetic–spin glass transition may be induced by increasing the antiferromagnetic bond concentration [44]. The origin of weak ferromagnetism in BFO could be understood by the displacement of oxygen ions which causes incomplete spin compensation in the two sublattices (interacting ferromagnetically within each sublattice) coupled antiferromagnetically. Moreover, the symmetry restriction for the Dzyaloshinskii–Moriya vector ' $\vec{D}$ ' is partially eliminated and the spins tend to rotate around that to minimize the energy,  $E_D = \vec{D} \cdot \vec{S}_i \times \vec{S}_j$ , where  $S_i$  and  $S_j$  are two neighbouring spins i.e.  $\text{Fe}^{3+}\text{--}\text{Fe}^{3+}$  or  $\text{Fe}^{3+}\text{--}\text{Ni}^{2+}$  [45]. But the energy minimization may not be achieved simultaneously for all the pairs, which causes variation in  $\vec{D}$  from site to site i.e., different internal canted magnetic structure. This may be the cause of the origination of various metastable states such as spin glass states [46].

To get an insight into spin dynamics the ESR measurements on BFO and BFNO samples were carried out. Figure 6 shows the room temperature ESR spectra of BFO and BFNO samples measured at 9.37 GHz. The spectra were found to be symmetric for all compositions. Only a single peak corresponding to the main mode or uniform precession mode is observed. A striking change in the spectrum of 5% Ni-doped sample is observed. This could be attributed to the slight change in the magnetic environment for the unpaired electrons of Fe. But, this effect is not prominent for higher % of Ni-doped samples. It is also noticed that, the resonant absorption field ( $H_r$ ) shifts towards low magnetic field with broader linewidth (presented in Table 1). The absence of any low/high frequency modes in these spectra, in addition to the main mode, indicates that samples are magnetically homogeneous.

The 'g' factors of the samples, were calculated using the relation,  $h\nu = g\mu_B H_r$ , where,  $\nu$  is the microwave frequency,

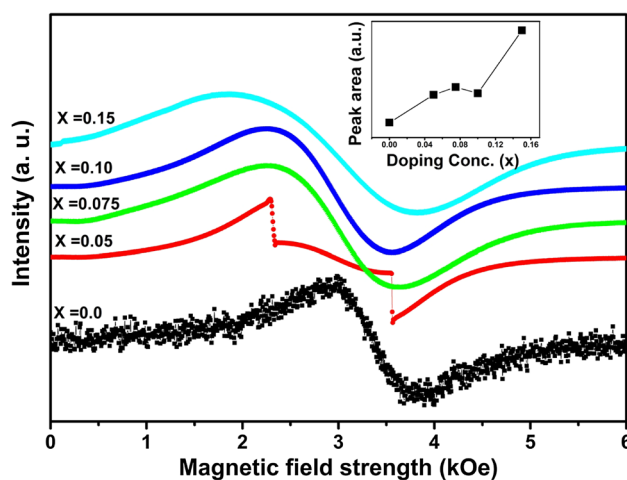


**Fig. 6** **a** Room temperature ESR spectra of  $\text{BiFe}_{1-x}\text{Ni}_x\text{O}_3$  ( $0.00 \leq x \leq 0.20$ ) samples, **b** variation of peak area with variation of doping concentration in  $\text{BiFe}_{1-x}\text{Ni}_x\text{O}_3$  ( $0.00 \leq x \leq 0.20$ ) samples

$h$  is the Planck's constant,  $\mu_B$  is the Bohr magnetron and  $H_r$  is the resonance magnetic field [47]. The BFO sample exhibited spectra at  $g \sim 1.99$ , which is an indication of the presence of  $\text{Fe}^{3+}$  ions only, is also confirmed from XPS studies. The  $H_r$  and the  $\Delta H$  are noticeably affected by adding even a low concentration (5%) of Ni. The  $g$ -values for BFNO samples  $g > 2$ , provide a strong evidence for the ferromagnetic coupling between  $\text{Fe}^{3+}\text{--}\text{Fe}^{3+}$  and  $\text{Fe}^{3+}\text{--}\text{Ni}^{2+}$ .

The peak area has been calculated as  $I(\Delta H)^2$ , where  $I$  is the peak-to-peak height [47] and is displayed as inset to Fig. 6. The peak area first increases with increasing  $x$  upto 0.075 and then showed a marginal decrease and thereafter a sharp increase for  $x=0.15$ . As the peak area is proportional to the number of spins participating in the resonance process, this confirms the increase in saturation magnetization (obtained from SQUID measurements) with increase in Ni concentration.

## 4 Conclusion

In conclusion, pristine BFO and BFNO ( $\text{BiFe}_{1-x}\text{Ni}_x\text{O}_3$ ) compounds were prepared by solid-state reaction route. The nickel doping has significantly influenced the properties without causing any structural distortion. XPS studies confirmed the presence of Fe in +3 oxidation state. Our magnetic measurements reveal that BFO has an antiferromagnetic response, with a trace of weak ferromagnetism. The nickel substitution decouples the antiferromagnetic interaction between the  $\text{Fe}^{3+}$  ions, which results into interactions between  $\text{Ni}^{2+}\text{--}\text{Fe}^{3+}$  and  $\text{Fe}^{3+}\text{--}\text{Fe}^{3+}$  ions with canting angle. This indicated the suppression of the helical order and creation of canted spin arrangements, which results in weak

**Table 1** Electron spin resonance parameters of BFO and BFNO samples measured at room temperature

Sl. no.	Samples	Observed value from experiment			Reported value in literature			References
		$H_r$ (Oe)	$\Delta H$ (Oe)	g	$H_r$ (Oe)	$\Delta H$ (Oe)	g	
1	BiFeO <sub>3</sub>	3407.70	909.09	1.99	2381.77	1806.86	2.81	Lin et al. [48]
2	BiFe <sub>0.95</sub> Ni <sub>0.05</sub> O <sub>3</sub>	3013.92	1278.59	2.25	–	–	–	
3	BiFe <sub>0.925</sub> Ni <sub>0.075</sub> O <sub>3</sub>	2987.36	1397.84	2.27	–	–	–	
4	BiFe <sub>0.9</sub> Ni <sub>0.1</sub> O <sub>3</sub>	2948.02	1290.32	2.30	–	–	–	
5	BiFe <sub>0.85</sub> Ni <sub>0.15</sub> O <sub>3</sub>	2910.43	1955.00	2.33	–	–	–	

ferromagnetism. The intrinsic properties could be biased by extrinsic effects, such as oxygen deficiency, presence of metastable states. The observed spin glass state at low temperature may be caused by the competition of the ferromagnetic and antiferromagnetic interaction in materials. This results in the existence of frustration and randomness in the ordering of the spins. The ac susceptibility measurements need to be carried out to determine the freezing point accurately. Moreover, the relation between the spin dynamics and microscopic behavior of these systems may be explored.

## References

1. T. Stevenson, D.G. Martin, P.I. Cowin, A. Blumfield, A.J. Bell, T.P. Comyn, P.M. Weaver, Piezoelectric materials for high temperature transducers and actuators. *J. Mater. Sci.* **26**(12), 9256 (2015)
2. M. Fiebig, Revival of the magnetoelectric effect. *J. Phys. D* **38**(R), 123 (2005)
3. K. Sharma, A. Singh, Advances in photovoltaic behaviour of ferroelectric BiFeO<sub>3</sub>. *J. Nanosci. Technol.* **2**(2), 85 (2016)
4. D. Moitra, C. Anand, B.K. Ghosh, M. Chondel, N.N. Ghosh, One-dimensional BiFeO<sub>3</sub> nanowire-reduced graphene oxide nanocomposite as excellent supercapacitor electrode material. *ACS Appl. Energy Mater.* **1**(2), 464 (2018)
5. S. Nayak, A. Soam, J. Nanda, C. Mahender, M. Singh, D. Mahapatra, R. Kumar, Sol-gel synthesized BiFeO<sub>3</sub>-graphene nanocomposites as efficient electrode for supercapacitor applications. *J. Mater. Sci.* **29**(11), 9361 (2018)
6. C. Yang, Y. Chen, W. Guo, Y. Gao, C. Song, Q. Zhang, N. Zheng, X. Han, C. Guo, Bismuth ferrite-based nanoplateform design: an ablation mechanism study of solid tumor and NIR-triggered photothermal/photodynamic combination cancer therapy. *Adv. Funct. Mater.* **28**(18), 1706827 (2018)
7. A.K. Pradhan, K. Zhang, D. Hunter, J.B. Dadson, G.B. Loutts, P. Bhattacharya, R. Katiyar, J. Zhang, D.J. Sellmyer, U.N. Roy, Y. Cui, A. Burger, Magnetic and electrical properties of single-phase multiferroic BiFeO<sub>3</sub>. *J. Appl. Phys.* **97**, 093903 (2005)
8. V.M. Gaikward, S.A. Acharya, Investigation on magnetic behaviour of BiFeO<sub>3</sub>: spin glass view point. *Adv. Mater. Lett.* **5**, 157–160 (2014)
9. J. Wang, J.B. Neaton, H. Zheng, V. Nagarajan, S.B. Ogale, B. Liu, D. Viehland, V. Vaithyanathan, D.G. Schlom, U.V. Waghmare, N.A. Spaldin, K.M. Rabe, M. Wuttig, R. Ramesh, Epitaxial BiFeO<sub>3</sub> multiferroic thin film heterostructures. *Science* **299**, 1719–1722 (2003)
10. G. Catalan, J.F. Scott, Physics and applications of bismuth ferrite. *Adv. Mater.* **21**, 2463–2485 (2009)
11. C. Fu, C. Long, W. Cai, G. Chen, X. Deng, Structural and magnetic properties of bismuth ferrite nanopowders prepared via Sol–Gel method. *Ferroelectrics* **460**, 157–161 (2014)
12. Y. Hu, L. Fei, Y. Zhang, J. Yuan, Y. Wang, H. Gu, Synthesis of bismuth ferrite nanoparticles via a wet chemical route at low temperature. *J. Nanomater.* 2011, 797639 (2011)
13. D. Zhang, P. Shi, X. Wu, W. Ren, Structural and electrical properties of sol–gel-derived Al-doped bismuth ferrite thin films. *Ceram. Int.* **39**, S461–S464 (2013)
14. Z. Ali, A. Atta, Y. Abbas, K. Sedeeq, A. Adam, E. Abdeltwab, Multiferroic BiFeO<sub>3</sub> thin films: structural and magnetic characterization. *Thin Solid Films* **577**, 124–127 (2015)
15. K. Chybezynska, P. Lawniczak, B. Hilczer, B. Leska, R. Pankiewicz, A. Pietraszko, I. Kepinski, T. Kaluski, P. Cieluch, F. Matelski, B. Andrzejewski, Synthesis and properties of bismuth ferrite multiferroic nanoflowers. *J. Mater. Sci.* **49**, 2596–2604 (2014)
16. A.M. Kadomtseva, A.K. Zvezdin, F. Yu, A.P. Popov Pyatakvo, G.P. Vorob'ev, Space–time parity violation and magnetoelectric interactions in antiferromagnets. *JETP Lett.* **79**, 571 (2004)
17. C. Ederer, N.A. Spaldin, Weak ferromagnetism and magnetoelectric coupling in bismuth ferrite. *Phys. Rev. B* **71**, 060401 (2005) R
18. M. Kumar, K.L. Yadav, Rapid liquid phase sintered Mn doped BiFeO<sub>3</sub> ceramics with enhanced polarization and weak magnetization. *Appl. Phys. Lett.* **91**, 242901 (2007)
19. B.C. Luo, C.L. Chen, Z. Xu, X. Xie, Effect of Cr substitution on the multiferroic properties of BiFe<sub>1-x</sub>Cr<sub>x</sub>O<sub>3</sub> compounds. *Phys. Lett. A* **374**, 4265–4268 (2010)
20. A. Kumar, K.L. Yadav, Magnetic, Magnetocapacitance and dielectric properties of Cr doped bismuth ferrite nanoceramics. *Mater. Sci. Eng. B* **176**, 227–230 (2011)
21. X. Qi, J. Dho, R. Tomov, M.G. Blamire, J.L.M. Driscoll, Greatly reduced leakage current and conduction mechanism in aliovalent-ion-doped BiFeO<sub>3</sub>. *Appl. Phys. Lett.* **86**, 062903 (2005)
22. A. Kumar, K.L. Yadav, The effect of Ni substitution on magnetic, dielectric and magnetoelectric properties in BiFe<sub>1-x</sub>Ni<sub>x</sub>O<sub>3</sub> system. *Phys. B* **405**, 4650–4654 (2010)
23. Y. Wang, G. Xu, L. Yang, Z. Ren, X. Wei, W. Weng, P. Du, G. Shen, G. Han, Enhancement of ferromagnetic properties in Ni-doped BiFeO<sub>3</sub>. *Mater. Sci. Pol.* **27**, 219–224 (2009)
24. Y.A. Chaudhary, C.M. Mahajan, P.P. Jagtap, S.T. Bendre, Structural, magnetic and dielectric properties of nano-crystalline Ni-doped BiFeO<sub>3</sub> ceramics formulated by self-propagating high-temperature synthesis. *J. Adv. Ceram.* **2**, 135–140 (2013)
25. Y.H. Wang, X. Qi, The effects of nickel substitution on bismuth ferrite. *Procedia Eng.* **36**, 455–461 (2012)
26. P. Kharel, S. Talebi, B. Ramachandran, A. Dixit, V.M. Naik, M.B. Sahana, C. Sudhaker, R. Naik, M.S.R. Rao, G. Lawes, Structural, magnetic, and electrical studies on polycrystalline transition-metal-doped BiFeO<sub>3</sub> thin films. *J. Phys.* **21**, 036001 (2009)

27. M.R. Biswal, J. Nanda, N.C. Mishra, S. Anwar, A. Mishra, Dielectric and impedance spectroscopic studies of multiferroic  $\text{BiFe}_{1-x}\text{Ni}_x\text{O}_3$ . *Adv. Mater. Lett.* **5**, 531–537 (2014)
28. K. Nakamoto, *Infrared and raman spectra of inorganic and coordination compounds*, 5th edn. (Wiley, New York, 1997)
29. S. Chakraborty, S. Mukherjee, S. Mukherjee, Effect of yttrium doping on the properties of bismuth ferrites: a review. *Int. J. Semicond. Sci. Technol.* **3**, 1 (2013)
30. D. Varshney, A. Kumar, K. Verma, Effect of yttrium doping on structural, thermal and dielectric properties of  $\text{BiFeO}_3$  ceramics. *J. Alloys Compd.* **509**, 8421 (2011)
31. B. Bhusan, Z. Wang, J.V. Tol, N.S. Dalal, A. Basumallick, N.Y. Vasanthacharya, S. Kumar, D. Das, Tailoring the magnetic and optical characteristics of nanocrystalline  $\text{BiFeO}_3$  by Ce doping. *J. Am. Ceram. Soc.* **1**, 8 (2012)
32. <http://xpspeak.software.informer.com/4.1/>
33. D.K. Mishra, X. Qi, Energy Levels and photoluminescence properties of Ni-doped bismuth ferrite. *J. Alloys Compd.* **504**, 27 (2010)
34. A.P. Grosvenor, B.A. Kobe, M.C. Biesinger, N.S. McIntyre, Investigation of multiplet splitting of Fe 2p XPS spectra and bonding in iron particles. *Surf. Interface Anal.* **36**, 1564 (2004)
35. S.T. Zhang, M.H. Lu, D. Wu, Y.F. Chen, N.B. Ming, Larger polarization and weak ferromagnetism in quenched  $\text{BiFeO}_3$  ceramics with a distorted rhombohedral crystal structure. *Appl. Phys. Lett.* **87**, 262907 (2005)
36. J. Xu, G. Wang, H. Wang, D. Ding, Y. He, Synthesis and weak ferromagnetism of Dy-doped  $\text{BiFeO}_3$  powders. *Mater. Lett.* **63**, 855 (2009)
37. J.-B. Li, G.H. Rao, J.K. Liang, Y.H. Luo, J. Luo, J.R. Chen, Magnetic properties of  $\text{Bi}(\text{Fe}_{1-x}\text{Cr}_x)\text{O}_3$  synthesized by a combustion method. *Appl. Phys. Lett.* **90**, 162513 (2007)
38. S.K. Pradhan, J. Das, P.P. Rout, V.R. Mohanta, S.K. Das, S. Samantaray, D.R. Sahu, J.L. Huang, S. Verma, B.K. Roul, Effect of holmium substitution for the improvement of multiferroic properties of  $\text{BiFeO}_3$ . *J. Phys. Chem. Solids* **71**, 1557 (2010)
39. K. Saravana Kumar, C. Venkataswaran, D. Kannan, B. Tiwari, M.S. Ramachandra Rao, Mechanical milling assisted synthesis of Ba–Mn Co-substituted  $\text{BiFeO}_3$  ceramics and their properties. *J. Phys. D* **45**, 415302 (2012)
40. Y.A. Chaudhary, C.M. Mahajan, P.P. Jagtap, S.T. Bendre, Structural, magnetic and dielectric properties of nano-crystalline Ni-doped  $\text{BiFeO}_3$  ceramics formulated by self-propagating high-temperature synthesis. *J. Adv. Ceram.* **2**, 135 (2013)
41. S.R. Das, R.N.P. Choudhary, P. Bhattacharya, R.S. Katiyar, P. Dutta, A. Manivannan, M.S. Seehra, Structural and multiferroic properties of La-modified  $\text{BiFeO}_3$  ceramics. *J. Appl. Phys.* **101**, 034104 (2007)
42. J. Iqbal, X. Liu, N. Ahmad, T. Harumoto, D. Yu, R. Yu, Room-temperature spin glass and near band edge properties of highly disorder  $(\text{FeCo})_{0.03}\text{Zn}_{0.97}\text{O}$  and  $(\text{FeCoNi})_{0.03}\text{Zn}_{0.97}\text{O}$  nanorods. *J. Appl. Phys.* **107**, 043902 (2010)
43. M.K. Singh, W. Prellier, M.P. Singh, R.S. Katiyar, J.F. Scott, Spin-glass transition in single-crystal  $\text{BiFeO}_3$ . *Phys. Rev. B* **77**, 144403 (2008)
44. G. Gulpnar, A.N. Berker, Quenched-vacancy induced spin-glass order. *Phys. Rev. E* **79**, 021110 (2009)
45. K. Eason, J.F. Kong, Z.W. Kho, C.H. Sim, M. Tran, J.C. Huang, M. Sabino, S.K. He, The effects of Dzyaloshinskii–Moriya interactions on the ferromagnetic resonance response in nanosized devices. *J. Appl. Phys.* **115**, 17C902 (2014)
46. M. Tovar, X. Obradors, F. Perez, S.B. Duro, J. Rivas, D. Chateigner, P. Bordet, J. Chenavas, Weak ferromagnetism and spin glass like behavior in  $\text{Tb}_2\text{CuO}_4$ . *J. Appl. Phys.* **70**, 6095 (1991)
47. L. Wu, C. Dong, H. Chen, J. Yao, C. Jiang, D. Xue, Hydrothermal synthesis and magnetic properties of bismuth ferrites nanocrystals with various morphology. *J. Am. Ceram. Soc.* **95**, 3922 (2012)
48. J.W. Lin, T. Tite, Y.H. Tang, C.S. Lue, Y.M. Chang, J.G. Lin, Correlation of spin and structure in doped bismuth ferrite nanoparticles. *J. Appl. Phys.* **111**, 07D910 (2012)